Hindawi
Geofluids
Volume 2020, Article ID 8834758, 16 pages
https://doi.org/10.1155/2020/8834758

Research Article

Fractal Characteristics of Pores in the Longtan Shales of Guizhou, Southwest China

Yuqi Huang,[1] **Peng Zhang**,[1] **Jinchuan Zhang**,[2] **Xuan Tang**,[2] **Chengwei Liu**,[1] **and Junwei Yang**[1]

[1]*School of Mining & Civil Engineering, Liupanshui Normal University, Liupanshui 553004, China*
[2]*School of Energy, China University of Geosciences (Beijing), Beijing 100083, China*

Correspondence should be addressed to Peng Zhang; zhangpeng8611@126.com

Received 24 July 2020; Revised 9 October 2020; Accepted 30 October 2020; Published 23 November 2020

Academic Editor: Zhouheng Chen

The pore structure of marine-continental transitional shales from the Longtan Formation in Guizhou, China, was investigated using fractal dimensions calculated by the FHH (Frenkel-Halsey-Hill) model based on low-temperature N_2 adsorption data. Results show that the overall $D1$ (fractal dimension under low relative pressure, $P/P_0 \leq 0.5$) and $D2$ (fractal dimension under high relative pressure, $P/P_0 > 0.5$) values of Longtan shales were relatively large, with average values of 2.7426 and 2.7838, respectively, indicating a strong adsorption and storage capacity and complex pore structure. The correlation analysis of fractal dimensions with specific surface area, average pore size, and maximum gas absorption volume indicates that $D1$ can comprehensively characterize the adsorption and storage capacity of shales, while $D2$ can effectively characterize the pore structure complexity. Further correlation among pore fractal dimension, shale organic geochemical parameters, and mineral composition parameters shows that there is a significant positive correlation between fractal dimensions and organic matter abundance as well as a complex correlation between fractal dimension and organic matter maturity. Fractal dimensions increase with an increase in clay mineral content and pyrite content but decrease with an increase in quartz content. Considering the actual geological evaluation and shale gas exploitation characteristics, a lower limit for $D1$ and upper limit for $D2$ should be set as evaluation criteria for favorable reservoirs. Combined with the shale gas-bearing property test results of Longtan shales in Guizhou, the favorable reservoir evaluation criteria are set as $D1 \geq 2.60$ and $D2 \leq 2.85$. When $D1$ is less than 2.60, the storage capacity of the shales is insufficient. When $D2$ is greater than 2.85, the shale pore structure is too complicated, resulting in poor permeability and difficult exploitation.

1. Introduction

Shale is a type of heterogeneous porous rock with a complex pore structure, including various pore shapes and sizes [1, 2]. Currently, the mercury intrusion method, adsorption-desorption method, and structural fractal method are commonly used to quantitatively analyze shale pore structure characteristics [3–5]. Pore fractal theory plays a significant role in studying the complexity of pore structures. The Permian Longtan Formation in Guizhou is a coal-bearing formation containing marine-continental transitional facies, which is generally characterized by high organic matter content and good gas indicators, indicating a great natural gas resource potential [6–9]. With the development of exploration and research, the evaluation of shale reservoirs has become an important research topic. Reservoir evaluation is one of the key steps to determining the natural productivity and economic value of shale reservoirs. Scientists have found that the Longtan Formation contains a set of shale reservoirs with low porosity (0.89%-2.29%) and permeability ($(0.16-29.5)\times10^{-4}$ mD), strong heterogeneity, small pore size, and complex pore structure [10]. Using qualitative methods such as polarized light microscopy and scanning electron microscopy, a qualitative understanding of the morphology and structure of the Longtan Formation has been gained [1, 10, 11]. However, there is limited quantitative research and evaluation of the Longtan Formation pore structure, and a geological parameter to characterize the pore structure well has not yet been identified and incorporated into the reservoir evaluation system. As a result, the pore structure is often neglected in the current reservoir evaluation system.

For conventional sandstone reservoirs, quantitative methods such as the mercury injection capillary pressure (MICP) experiment can be used to study pore structure characteristics [2, 12, 13]. Tight reservoirs, such as shale reservoirs, have high pore displacement pressure, requiring a higher experiment pressure to measure the pore size. However, high-pressure mercury injection can damage the pore structure of shale [14]. To address this problem, fractal theory, which is an effective approach for studying the irregular surface and heterogeneity of porous materials, was introduced into the study of shale pores [14–18]. Fractal theory considers the complicated pore fracture as a whole and quantitatively evaluates the heterogeneity and irregular surface of pores in shale reservoirs [5, 9].

Therefore, this paper systematically studied the pore structures and fractal characteristics of marine-continental transitional facies shales in Guizhou as well as the relationship with other geological parameters (reservoir parameters, organic geochemical parameters, and mineral composition parameters) based on low-temperature N_2 adsorption experiments, field emission scanning electron microscopy (FE-SEM) observations, X-ray diffraction (XRD) analysis of rock mineral composition, organic geochemical experiments, and gas content tests. In this study, the characterization function and geological significance of fractal dimension on pore structure are clarified. Also, the fractal dimension division standard is determined for the dominant shale reservoirs of the Longtan Formation in Guizhou Province, which provides the basis for further exploration, research, and evaluation.

2. Geological Conditions for Shale Development

The main portion of the study area is located in the Qianzhong Uplift and the depression in the northern Dianqian area, belonging to the Upper Yangtze plate (Figure 1). The regional structure is characterized by NNE-trending and NE-trending folds and faults. The study area is intersected by the Hezhang—Zunyi NE-trending fault to the north and surrounded by the Nayong fault to the southeast [19, 20]. Since the formation of the continent in the Middle Permian, the crust has been exposed and eroded. The Longtan Formation, a coal-bearing series of marine-continental sedimentary strata, has been widely deposited in northwest Guizhou. The alternating sedimentary facies combinations, including lagoon facies, tidal-control delta facies, tidal-flat facies, and peat swamp facies, were developed during the Longtan Period [21]. The shale has a small single layer thickness but large cumulative thickness, containing multiple interlayers and coal seams [20, 22]. The lithology is dominated by black carbon shale, silty mudstone, sandstone, siltstone, marlite, and coal (Figure 1).

3. Samples and Experimental Methods

Samples in this study are all unweathered Longtan core samples from Well-XY1 (X-1 to X-6 in Table 1), Well-FY1 (F-1to F-3 in Table 1), and Well-JS1 (the locations of the three wells are shown in Figure 1). All samples were taken from gas-bearing layers and contain the primary Longtan shale reservoir lithology. The depth and lithology of the samples are listed in Tables 1 and 2.

A complete experimental project was conducted, including measurements of organic carbon (TOC) content, kerogen microcomponents, vitrinite reflectance (R_o), XRD analysis of rock mineral composition, argon ion polishing—field emission scanning electron microscopy, low-temperature N_2 adsorption, isothermal adsorption, and gas content analyses (direct method).

The TOC tests were conducted using a LECO-CS230 carbon and sulfur analyzer. The powder samples (100 mg) were treated with 5% HCl (hydrochloric acid) at 80°C to remove inorganic carbon and then washed with pure water to remove residual HCl. The treated samples were placed into the apparatus to measure TOC content. The experiments conformed to the national standard GB/T19145-2003 (No. GB/T19145-2003 of the National Standards of the People's Republic of China). An Axio Scope A1 microphotometer was used to measure R_o with SY/T5124-2012 and SY/T5125-2014 as the test bases (No. SY/T5124-2012 and SY/T5125-2014 of the Petroleum Industry Standard of the People's Republic of China).

An X'Pert Powder X-ray diffractometer (PANalytical Company, Netherlands) was used to measure the mineralogical compositions of the Longtan Shale samples. Samples were crushed into powders with grain size ranging from 200 to 300 mesh before the XRD analysis. The experiments conformed to the industry standard SY/T5163-2010.

Samples were polished by Argon ion using an Ilion II697 argon-ion polisher (Gatan Company). Then, the polished samples were scanned using a Merlin Compact field emission scanning electron microscope (ZEISS Company) to obtain the micromorphology images with an acceleration voltage of 10.0 kV and working distance ranging from 2 to 15 mm. The experiments conformed to the industry standard GB/T 16594-2008 and SY/T 5162-1997.

Low-temperature N_2 adsorption experiments were performed using a Quadrasorb SI specific surface analyzer. The crushed samples (60-80 mesh) were degassed for 4 h at 150°C. Then, N_2 adsorption experiments were conducted at -196°C under a relative pressure ranging from 0.040 to 0.997. The specific surface area and average pore size were calculated using the Brunauer-Emmett-Teller (BET) method (Brunauer et al., 1938). The experiments conformed to the industry standard GB/T19587-2004.

Isothermal adsorption tests were conducted using a GAI-100 high-pressure gas isothermal adsorption apparatus with a pressure range of 0.007-17.300 MPa at 30°C with SY/T 6132-1995 as the test basis. The desorbed gas content and residual gas content data were directly measured using a tubeless field desorption instrument and a fully sealed residual gas analyzer independently developed by the China

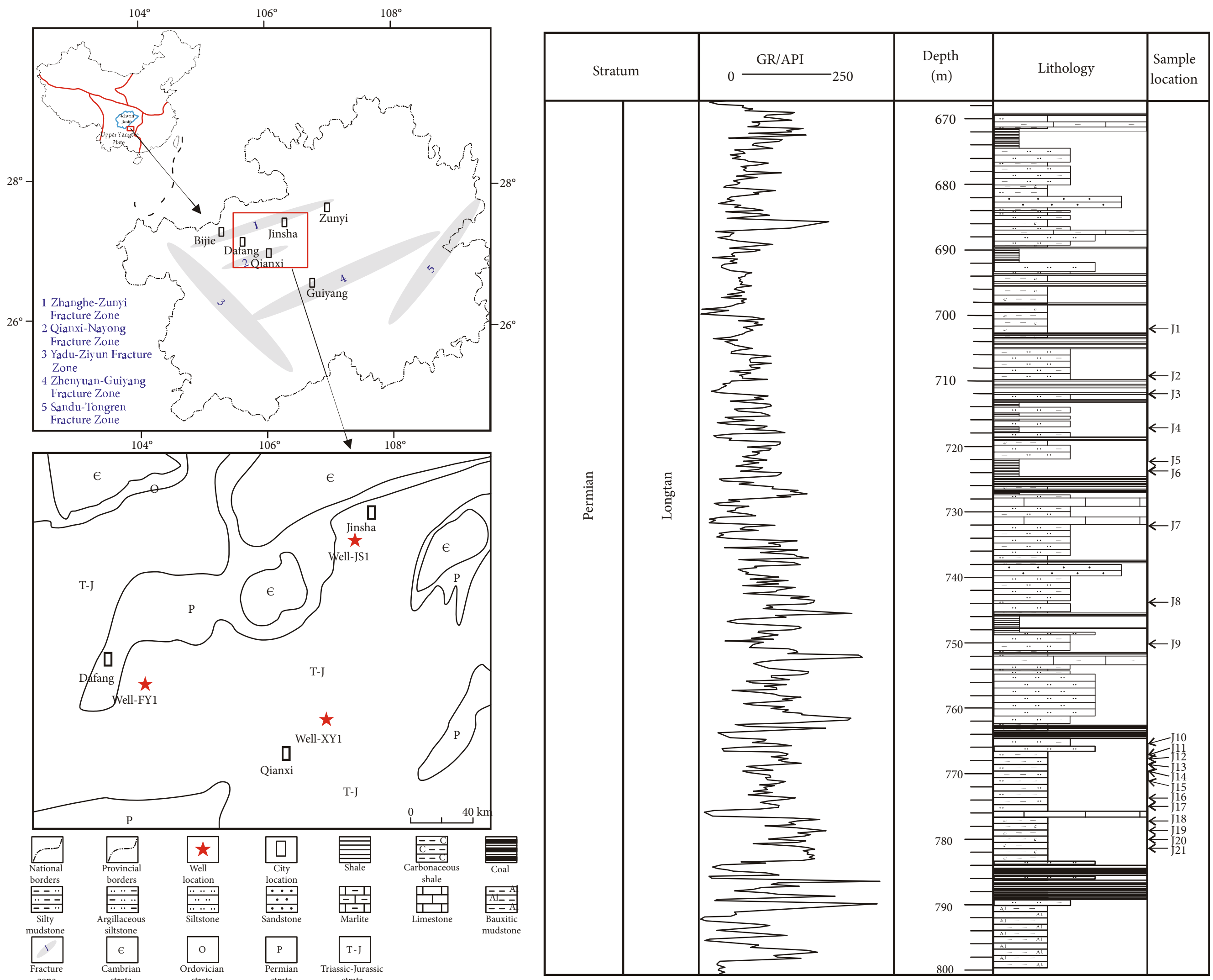

Figure 1: Geological background of the research area and stratigraphic column of the Longtan Formation.

University of Geosciences (Beijing). The lost gas content was obtained by mathematical calculation. ISO18871-2015 was used as the reference standard.

4. Results

4.1. Reservoir Characteristics. According to the geochemical test results from Longtan shale samples, the TOC of shales ranges from 1.01% to 8.62%, with an average value of 3.68%, indicating that the overall organic matter content is relatively high. R_o values primarily range from 2.00% to 3.00% with an average value of 2.61% (Table 1), indicating that Longtan shale is in the early overmature stage with good gas generation conditions. Longtan shales are primarily composed of quartz, feldspar, carbonate minerals, and clay minerals. The quartz content ranges from 10.46% to 38.19% with an average value of 28.99%, and clay mineral content ranges from 25.94% to 47.37% with an average value of 40.37%, which is relatively large. In addition, clay minerals are primarily composed of illite/montmorillonite and illite, while chlorite, kaolinite, and montmorillonite account for a small proportion (Table 1).

Through FE-SEM observations, Longtan shale pores can be divided into four types: inorganic intergranular pores, inorganic intragranular pores, organic pores, and microfractures based on their relationships with grain and pore morphology. Inorganic intergranular pores are mostly intercrystalline pores and shrink fractures along the grain (Figures 2(a) and 2(f)), with large pore sizes ranging from mesopores (2-50 nm) to macropores (≥50 nm). With simple structure and good connectivity, inorganic pores are primarily intercrystalline pores between clay minerals and dissolution pores (Figures 2(b) and 2(c)). The intercrystalline pores of clay minerals are mostly slit-shaped with good connectivity, and dissolution pores are mostly round or irregular with relatively poor connectivity, including both micropores (<2 nm) and macropores. Both the organic abundance and maturity can control the development of organic pores. In the Guizhou area, Longtan shales have high organic abundance, and the maturity is primarily in the early overmature stage. Organic pores are mostly round and elliptical in shape

Table 1: Organic geochemistry and mineral composition test results of Longtan shales.

Sample	Depth/(m)	Lithology	TOC/(%)	R_o/(%)	Clay mineral content/(%)	Quartz content (%)	Carbonate mineral content/(%)	Feldspar content/(%)	Pyrite content/(%)	Clay mineral composition: Kaolinite content/(%)	Chlorite content/(%)	Montmorillonite content/(%)	Illite content/(%)	Illite/montmorillonite mixed layer content/(%)
J-2	709.3	Argillaceous siltstone	1.84	2.61	/	/	/	/	/	/	/	/	/	/
J-3	712.4	Shale	2.52	2.34	/	/	/	/	/	1	5	0	0	94
J-4	717.3	Shale	/	3.16	/	/	/	/	/	/	/	/	/	/
J-5	722.7	Shale	6.88	2.78	42.03	33.87	13.91	10.2	/	1	7	0	68	24
J-6	723.7	Shale	/	/	44.75	35.02	8.42	11.8	/	1	4	0	0	95
J-8	743.7	Silty mudstone	/	/	38.22	28.83	21.55	11.4	/	2	12	0	0	86
J-9	750.8	Argillaceous siltstone	1.86	/	/	/	/	/	/	/	/	/	/	/
J-10	765.2	Argillaceous siltstone	1.96	/	25.94	25.54	0	13.1	/	1	5	13	81	0
J-13	768.3	Silty mudstone	2.31	2.32	37.43	36.65	9.72	12.5	/	3	3	0	94	0
J-14	769.6	Silty mudstone	2.13	/	36.8	38.19	14.45	6.89	3.68	10	10	2	78	0
J-15	771.3	Silty mudstone	/	/	/	/	/	/	/	/	/	/	/	/
J-16	774.2	Silty mudstone	1.36	2.17	/	/	/	/	/	/	/	/	/	/
J-18	777	Shale	5.89	/	47.85	29.12	2.26	0	20.78	/	/	/	/	/
J-19	778.7	Shale	6.99	/	/	/	/	/	/	7	9	0	0	84
J-20	780	Shale	8.7	/	43.51	22.27	5.11	0	29.11	0	0	100	0	0
J-21	781.3	Shale	8.62	2.42	47.37	24.41	0	0	28.22	1	2	0	0	97
F-1	983	Silty mudstone	3.3	2.15	39.74	10.46	0	40.98	/	12	23	0	54	/
F-2	1016	Shale	3.48	2.32	34.06	30.36	7.14	3.34	/	7	11	0	62	/
F-3	1024	Shale	1.85	2.44	46.71	33.17	2.75	9.8	/	6	21	0	46	/
X-1	481	Shale	2.52	/	/	/	/	/	/	/	/	/	/	/
X-2	420	Shale	2.86	2.81	/	/	/	/	/	/	/	/	/	/
X-3	430	Shale	5.23	2.72	/	/	/	/	/	/	/	/	/	/
X-4	399	Shale	2.34	/	/	/	/	/	/	/	/	/	/	/
X-5	518	Silty mudstone	1.01	3.16	/	/	/	/	/	/	/	/	/	/
X-6	470	Shale	/	3.16	/	/	/	/	/	/	/	/	/	/

Note: /: no experiments or no results.

Table 2: Fractal dimensions and gas content test results of Longtan shales.

Sample	Depth/(m)	Lithology	D1	$R^2$1	D2	$R^2$2	BET specific surface area/(m^2■g^{-1})	Average pore size/(nm)	Desorption gas content/(m^3/t)	Lost gas content/(m^3/t)	Residual gas content/(m^3/t)	Maximum adsorption capacity/(m^3/t)
J-1	702.2	Shale	2.677	0.9997	2.7096	0.9952	9.77	7.82	/	/	/	/
J-2	709.3	Argillaceous siltstone	2.6709	0.9992	2.6845	0.9925	11.8	8.46	/	/	/	/
J-3	712.4	Shale	2.6882	0.9986	2.7047	0.9892	14.47	7.11	/	/	/	1.4987
J-4	717.3	Shale	2.6655	0.9997	2.7001	0.9978	10.85	7.68	0.45	0.012	1.469	/
J-5	722.7	Shale	2.7374	0.9978	2.7934	0.9853	18.76	5.26	/	/	/	/
J-6	723.7	Shale	2.7564	0.9967	2.787	0.9937	13.52	5.46	/	/	/	/
J-7	731.9	Argillaceous siltstone	2.7353	0.9918	2.8135	0.9849	19.02	4.86	0.53	0.017	1.515	/
J-8	743.7	Silty mudstone	2.7674	0.9951	2.8356	0.9759	9.366	4.42	/	/	/	/
J-9	750.8	Argillaceous siltstone	2.7368	0.9974	2.7826	0.9633	12.09	6.12	/	/	/	/
J-10	765.2	Argillaceous siltstone	2.7002	0.9976	2.7513	0.9867	11.29	5.92	/	/	/	/
J-11	766.7	Silty mudstone	2.7447	0.9953	2.7759	0.9897	16.21	5.33	0.59	0.009	1.61	1.662
J-12	767.1	Silty mudstone	2.7521	0.9953	2.774	0.9901	16.84	5.59	/	/	/	1.6620
J-13	768.3	Silty mudstone	2.7326	0.9951	2.7647	0.9833	16.12	5.71	0.54	0.006	1.441	/
J-14	769.6	Silty mudstone	2.68	0.9985	2.76	0.9868	10.87	6.61	/	/	/	/
J-15	771.3	Silty mudstone	2.7356	0.9941	2.7845	0.9891	15.25	5.2	/	/	/	/
J-16	774.2	Silty mudstone	2.724	0.9971	2.7423	0.9889	9.511	6.16	/	/	/	1.4165
J-17	775.4	Silty mudstone	2.6789	0.9972	2.6841	0.9909	8.315	7.94	0.48	0.005	1.769	/
J-18	777	Shale	2.8637	0.9679	2.9256	0.9932	21.88	2.72	0.68	0.028	1.768	3.074
J-19	778.7	Shale	2.8648	0.9786	2.906	0.9941	29.45	2.96	0.66	0.013	1.877	/
J-20	780	Shale	2.8249	0.9886	2.8638	0.9926	25.2	3.63	/	/	/	/
J-21	781.3	Shale	2.8583	0.9797	2.9171	0.9812	31.18	2.87	/	/	/	2.8538

Note: $R^2$1: correlation coefficient of *D*1; $R^2$2: correlation coefficient of *D*2; BET: Brunauer-Emmett-Teller; /: no experiments or no results.

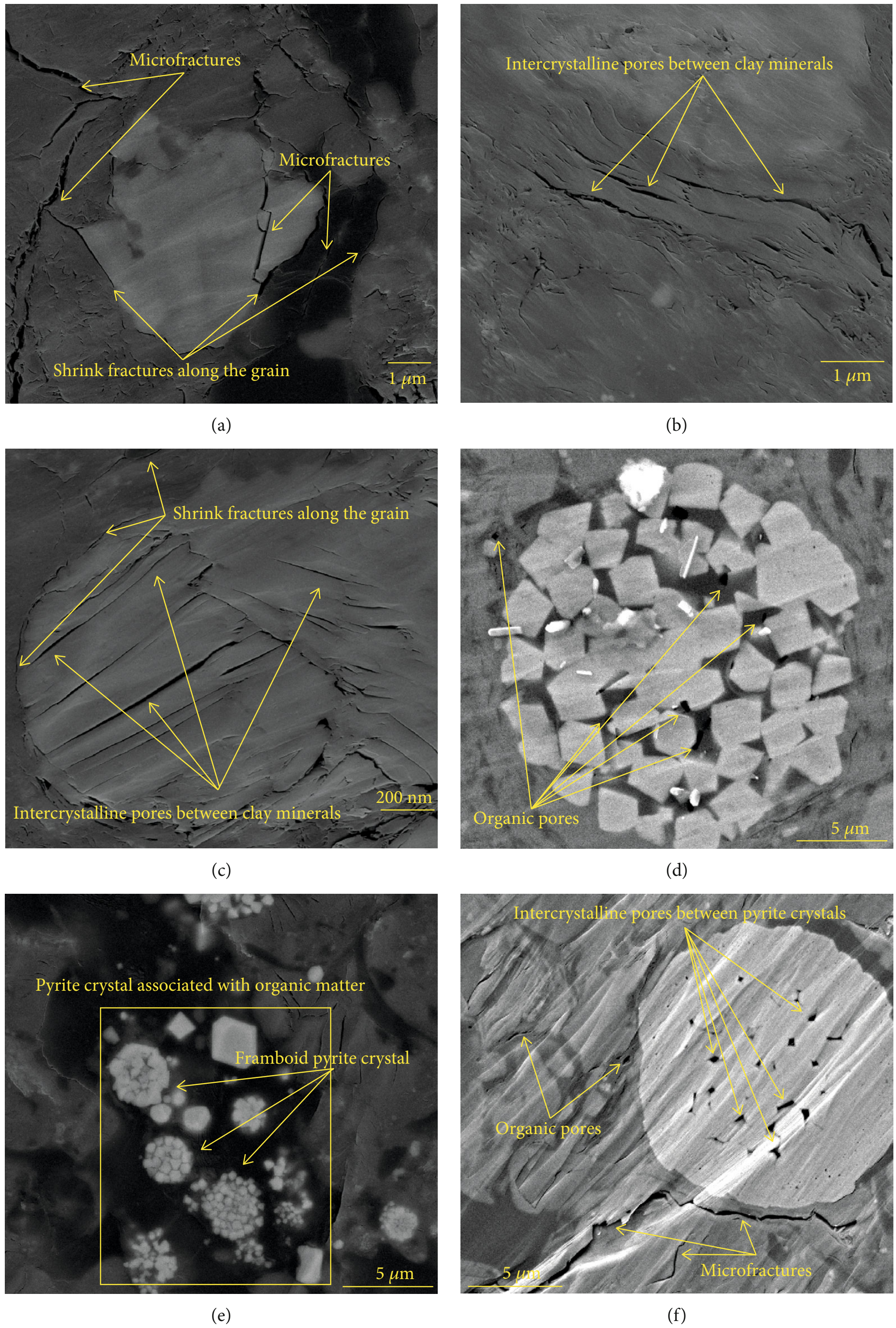

Figure 2: Continued.

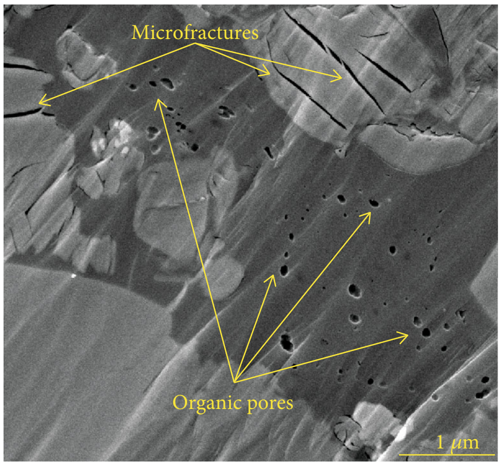

(g)

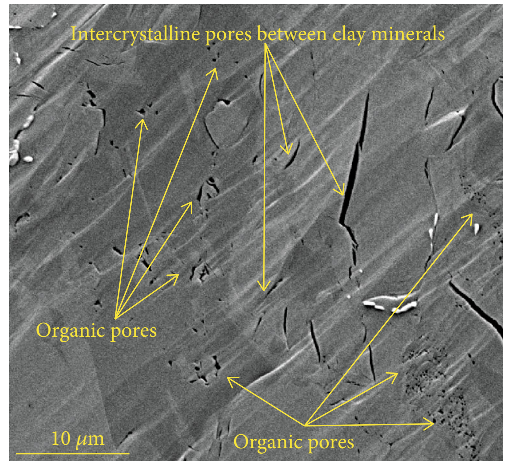

(h)

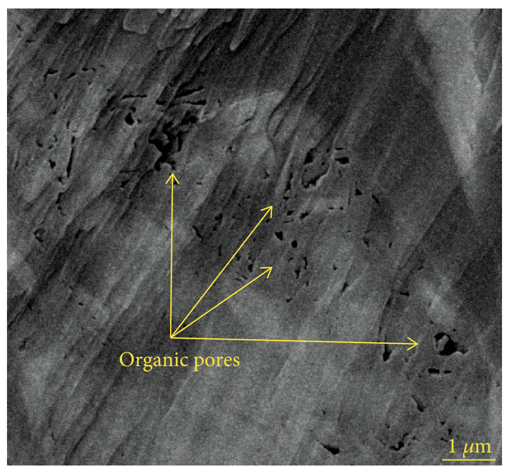

(i)

Figure 2: FE-SEM images of pores in Longtan shale samples ((a) sample from Well-XY1, 430.0 m, black carbonaceous shale; (b) sample from Well- XY1, 443.5 m, black carbonaceous shale; (c) sample from Well- XY1, 430.0 m, black carbonaceous shale; (d) sample from Well-JS1, 751.0 m, dark grey silty mudstone; (e) sample from Well-XY1, 439.0 m, black carbonaceous shale; (f) sample from Well-JS1, 781.4 m, black carbonaceous shale; (g) sample from Well-JS1, 781.4 m, black carbonaceous shale; (h) sample from Well-JS1, 779.3 m, black carbonaceous shale; (i) sample from Well-JS1,781.4 m, black carbonaceous shale).

with relatively poor connectivity (Figures 2(g), 2(h), and 2(i)), including both micropores and macropores. Microfractures are most likely related to tectonic activity and commonly appear within brittle mineral crystals (Figures 2(a), 2(g), and 2(h)). They play an important role in increasing pore connectivity and improving the reservoir properties of the Longtan Formation.

Low-temperature N_2 adsorption-desorption experiments show that the specific surface area of Longtan shales ranges from 8.32-31.18 m^2/g (average 15.79 m^2/g). The proportion of micropores is high, primarily distributed from 3 nm to 5 nm (Figure 3), but there are also some mesopores and macropores larger than 25 nm. Adsorption-desorption curves show that the adsorption volume of the Longtan shales in the low-pressure region is small, and the slopes of the curves vary without any significant inflection points. The higher the relative pressure is, the larger the adsorption volume is. Capillary condensation of the adsorbate occurs, and the isotherm rises rapidly. Desorption lag occurs due to the capillary force. According to the IUPAC classification [23–28], the increasing hysteresis is H2 type and H3 type (Figure 4), indicating that quite a few flaky grains, primarily clay minerals, are present within the shale. Pores are primarily slit, wedge, and ink bottle-shaped [4, 11, 26].

4.2. Shale Pore Fractal Dimension. Pore fractal dimensions were calculated based on the fractal FHH (Frenkel-Halsey-Hill) model using low-temperature N_2 adsorption data for the Longtan shale (Table 2) [26, 28–30]. The calculation formula is

$$\mathrm{Ln}V = \mathrm{const} + (D - 3) \times \mathrm{Ln}\left[\mathrm{Ln}\left(\frac{P_0}{P}\right)\right], \quad (1)$$

where V—the volume of adsorbed gas at the equilibrium pressure P, cm^3/g; P_0—saturated vapor pressure, MPa; P—equilibrium pressure, MPa; D—fractal dimension.

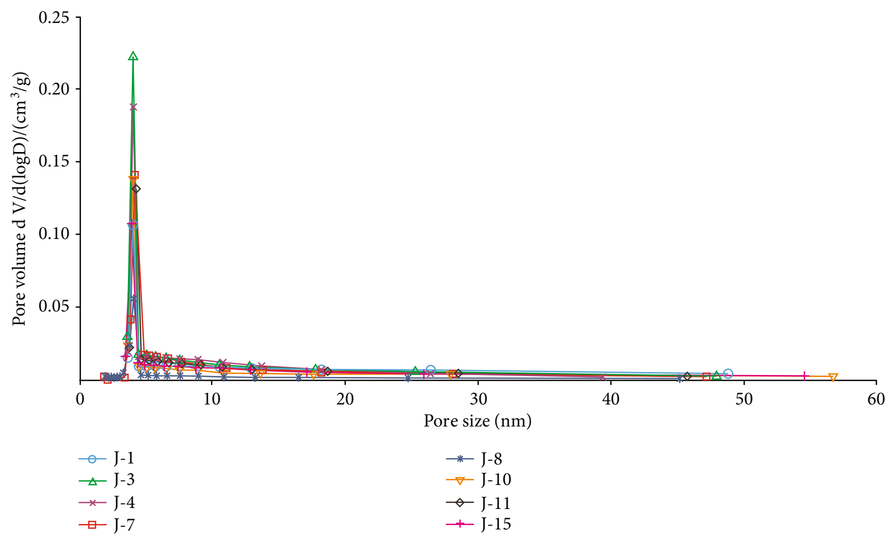

FIGURE 3: Pore size distribution characteristics of Longtan shales.

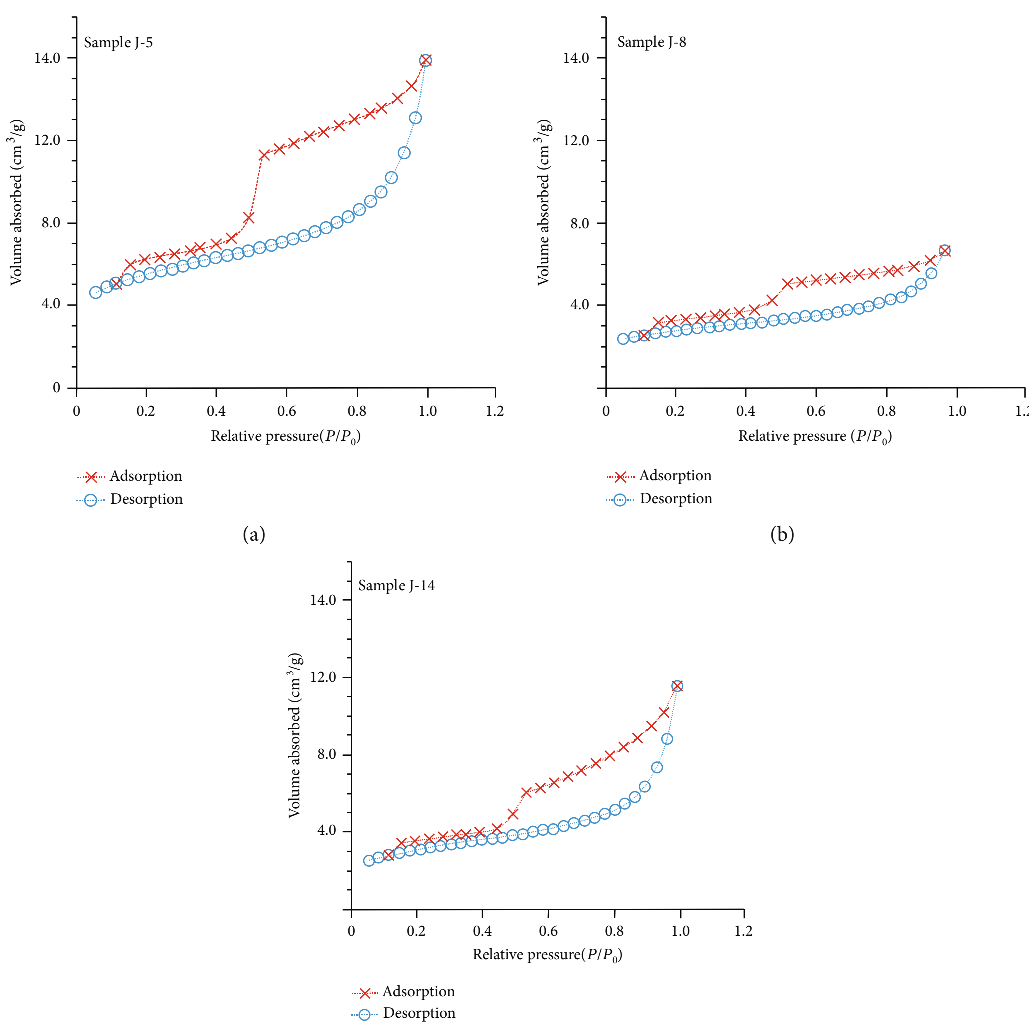

FIGURE 4: N_2 adsorption-desorption isotherms of Longtan shales (P_0—saturated vapor pressure, MPa; P—equilibrium pressure, MPa).

According to the fractal FHH model, D (fractal dimension) can be determined by the slope of the fitting line in the plot of $\mathrm{Ln}V - \mathrm{Ln}[\mathrm{Ln}(P_0/P)]$. Generally, D ranges from 2 to 3 [31, 32]. When D is closer to 2, the pore structure is simple with a smooth and regular surface. On the other hand, when D is closer to 3, the pore structure is complex with an irregular surface, strong heterogeneity, and strong fluid flow resistance. A high fractal dimension usually means a complex pore structure, which is more favorable for gas adsorption and storage than for gas transport [25, 26].

The piecewise least-square fitting line obtained from the experimental data reflects two different fractal characteristics in the shale pores (Table 2) (Figure 5). The fractal dimension value calculated using a curve with relatively low pressure ($P/P_0 \le 0.5$) was recorded as $D1$, and the fractal dimension calculated using a curve with relatively high pressure was recorded as $D2$ ($P/P_0 > 0.5$). The plots of $\ln(V)$ versus $\ln[\ln(P_0/P)]$ are shown in Figures 5 and 6. $D1$ ranges from 2.6655 to 2.8648 with an average value of 2.7426, and $D2$ ranges from 2.6841 to 2.9256 with an average value of 2.7838. $D1$ and $D2$ are large and close to 3. Also, $D2$ is greater than $D1$ (Figure 6).

5. Discussion

5.1. Characterization Function of Fractal Dimensions. The correlation between the calculated fractal dimensions and the specific surface area (Figure 7(a)) as well as the average pore size (Figure 7(b)) is examined to determine the fractal dimension characterization function of the pore structures and shale storage properties. $D1$ and $D2$ increase with the increase in specific surface area and decrease in pore size. The correlation between $D1$ and specific surface area is slightly better than that of $D2$, while the correlation between $D2$ and average pore size is slightly better than that of $D1$. $D1$ is more effective for comprehensively characterizing the shale adsorbed gas storage capacity, while $D2$ can effectively characterize pore structure complexity and reservoir heterogeneity. Shale isothermal adsorption tests showed that the maximum adsorption gas volume has a significant positive correlation with $D1$ (Figure 7(c)), which further verifies the ability of $D1$ to characterize the gas adsorption and storage capacity of shales. According to the $D1$ and $D2$ values for the marine-continental transitional facies Longtan shales in the Guizhou area, the overall adsorbed gas adsorption and storage capacity is good, indicating that the Longtan shales are a good reservoir for adsorbed natural gas. However, the pore size is small, and the pore structure is complex with relatively poor connectivity.

5.2. Relationship between Fractal Dimensions and Organic Geochemical Characteristics. Shale is typically rich in organic matter. The nanomicroorganic pores present in the organic matter are important storage spaces for gas [22, 33, 34]. Therefore, a significant relationship exists between the organic geochemical characteristics and fractal dimensions. By analyzing the correlation between fractal dimensions and TOC (Figure 8(a)) as well as R_o (Figure 8(b)), it is found that a good positive correlation exists between fractal dimensions and TOC. The fractal dimensions increase with increasing organic matter abundance because the organic pores and clay mineral-related inorganic pores are the most important type of shale reservoirs. In marine-continental transitional facies shales, organic matter is commonly associated with clay minerals, indicating that both organic pores and inorganic pores are well developed in organic-rich shales. All these pores have small diameters and complex structures resulting in a significant increase in fractal dimensions. The correlation between fractal dimensions and R_o is not obvious. The fitting lines show that when R_o ranges from 2.0-2.5%, fractal dimensions increase with increasing R_o. $D1$ and $D2$ both reach the peak when R_o is around 2.5%, then fractal dimensions show a negative correlation with R_o. However, the two fitting line confidences are low, because the type-III kerogen is still in thermal pyrolysis in the early overmature stage, and organic pores can be developed along with gas generation. The development of the organic pores determines the increase in fractal dimensions. However, along with this process, the graphitization of organic matter also occurs [35], which reduces the adsorption capacity of shales and even collapses the graphitized organic pores. Under the simultaneous influence of these two effects, the fractal dimension and the organic maturity show a complicated relationship. The specific change trend of the fractal dimensions is related to the relative strength of these two effects. When the thermal pyrolysis gas generation dominates, fractal dimensions increase. Conversely, when graphitization dominates, fractal dimensions decrease.

5.3. Relationship between Fractal Dimensions and Mineral Components. As different minerals develop pores with different structures, the mineral composition of shales is also an important factor influencing fractal dimensions. Quartz and clay minerals are the primary minerals within the Longtan shales. Fractal dimensions are negatively correlated with quartz content (Figure 9(a)) because the Longtan Formation is a set of marine-continental transitional shales, and the quartz contained therein is primarily terrestrial quartz. Therefore, organic abundance is negatively correlated with quartz content (Figure 10). Furthermore, the grain size of quartz minerals is relatively large. Hence, pores related to quartz are intergranular pores and microfractures (macropores to mesopores) with simple structures. The increase in the quartz content results in an increase in simple macropores in shales, causing a decrease in fractal dimensions. On the contrary, fractal dimensions have a good positive correlation with clay mineral content (Figure 9(b)). As previously mentioned (Section 4.2), the organic abundance in marine-continental transitional shales is positively correlated with clay mineral content (Figure 10), indicating that shales rich in clay minerals are also organic-rich. Thus, inorganic as well as organic micropores with complex structures can be developed in these shales. Shales rich in clay minerals have strong gas adsorption and storage capacity, with complex pore structures and strong heterogeneity with large fractal dimensions. In addition to quartz and clay content, pyrite content also has a significant effect on the fractal dimension (Figure 9(c)). Numerous studies have shown that pyrite

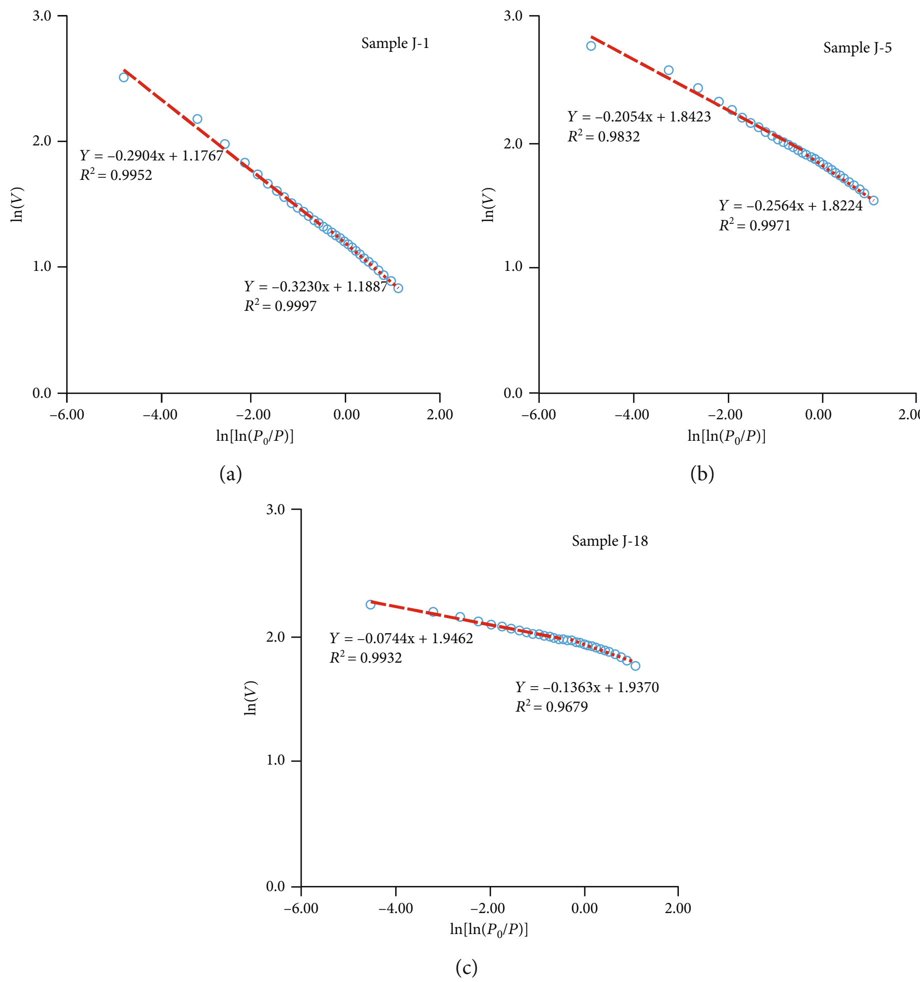

FIGURE 5: Fitting lines of pore fractal dimensions for Longtan shales.

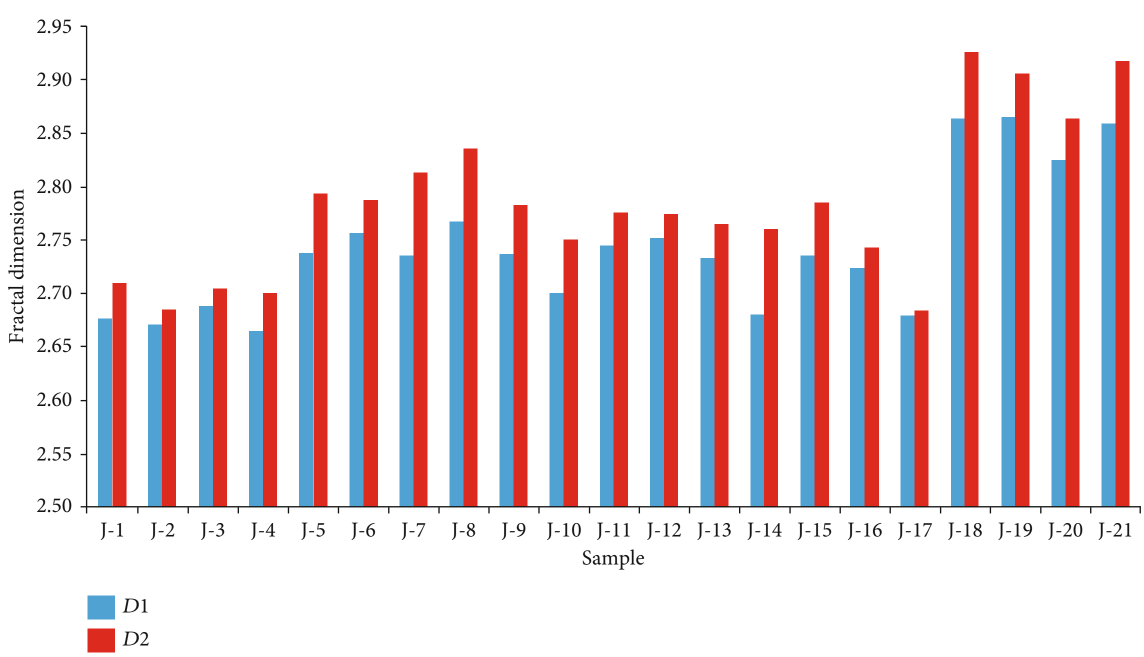

FIGURE 6: Fractal dimensions of Longtan shales.

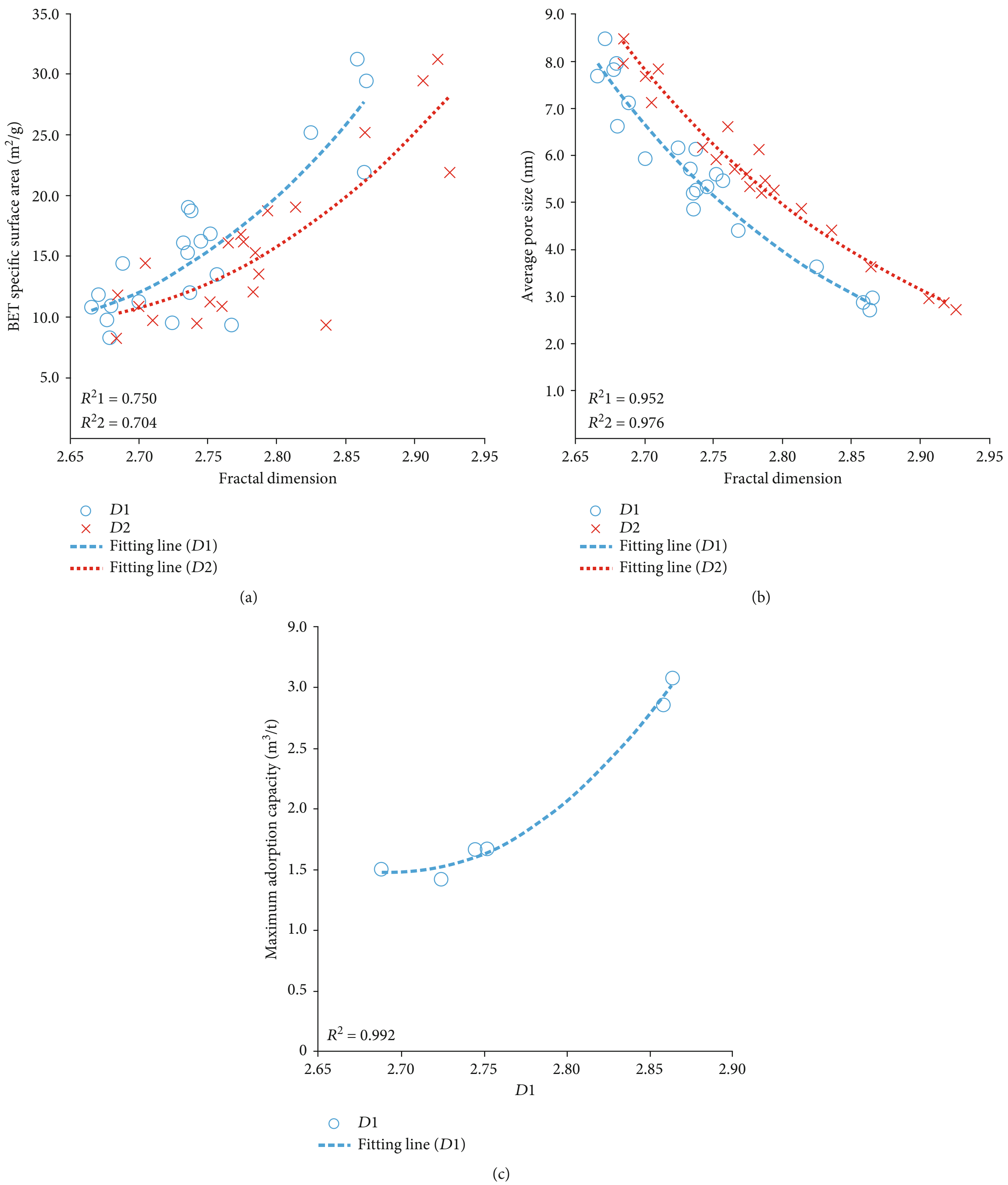

Figure 7: Correlation among BET specific surface (a), average pore size (b), adsorption capacity (c), and fractal dimensions of Longtan shales.

primarily develops in an oxygen-deficient environment, which is conducive to the preservation of organic matter [6, 36–38]. Organic abundance shows a good positive correlation with pyrite content (Figure 10). Framboid pyrites, a type of pyrite which predominantly influences pore structures [39, 40], are the primary type found in Longtan shales. Intercrystalline pores are developed inside framboid pyrites and are commonly filled with organic matter (Figures 2(d) and 2(e)). Pyrite crystals can serve as supporting frameworks to protect organic matter and organic pores within them [22, 36, 41, 42]. Therefore, the shale samples with large pyrite content in this study contain abundant organic matter and

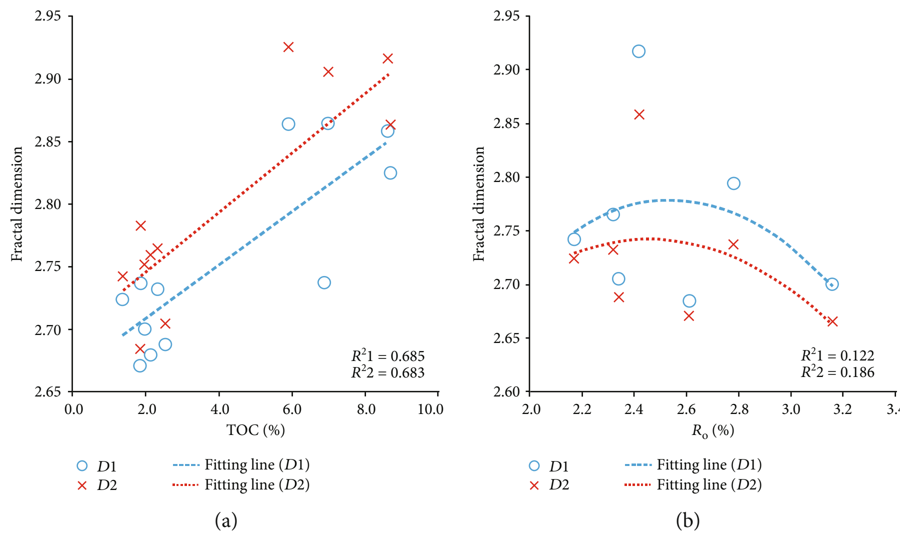

Figure 8: Correlation among fractal dimensions and geochemical parameters of Longtan shales.

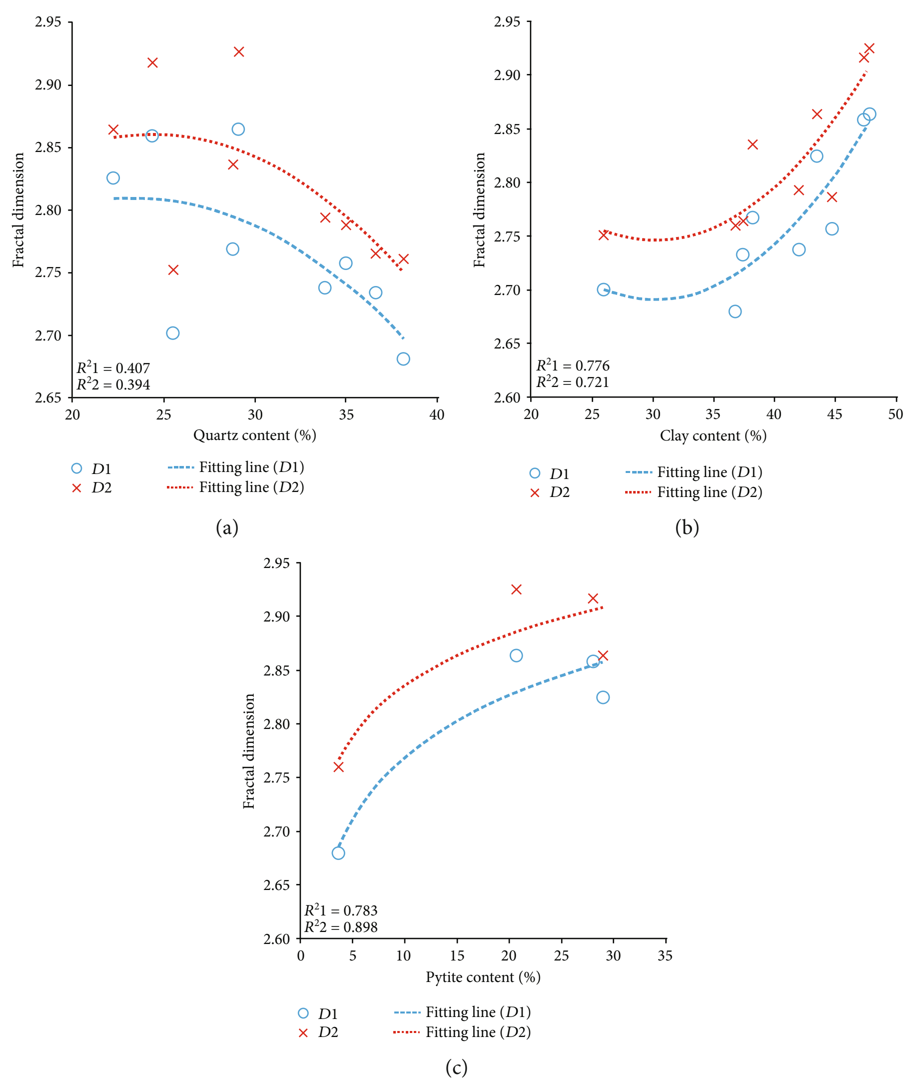

Figure 9: Correlation between fractal dimensions and mineral content of Longtan shales.

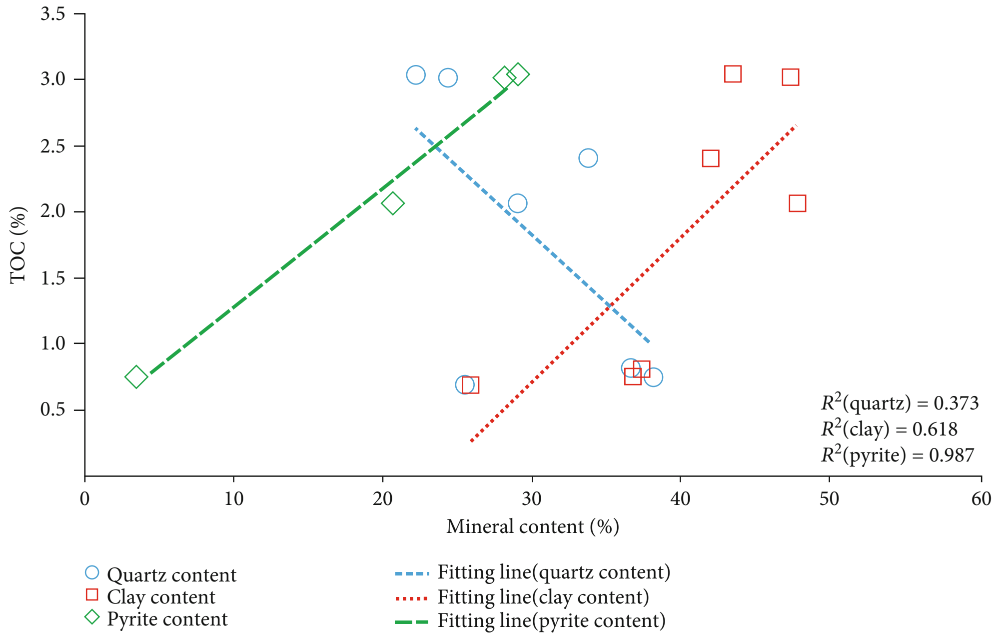

FIGURE 10: Correlation between organic abundance and mineral content of Longtan shales.

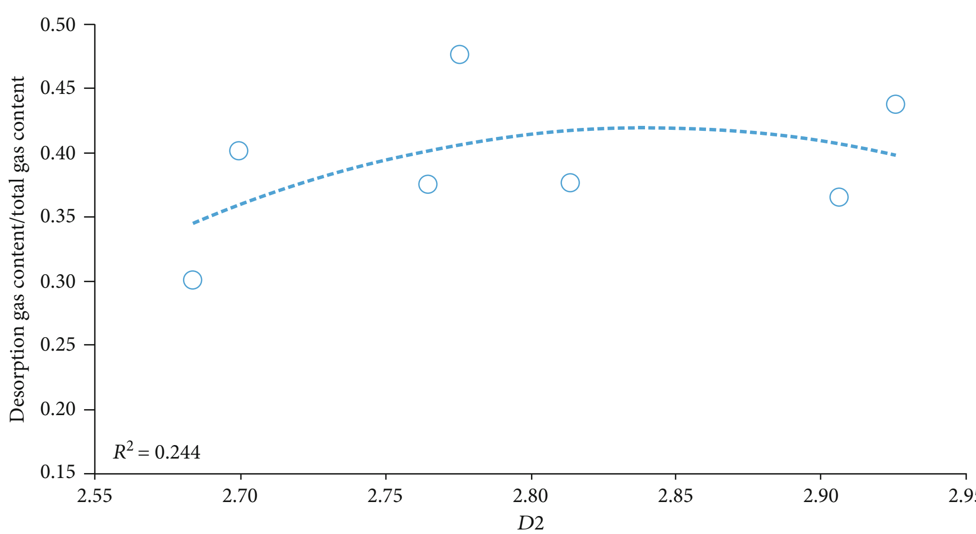

FIGURE 11: Correlation between gas-bearing composition and fractal dimensions of Longtan shales.

well-developed organic pores, thus having a large fractal dimension.

6. Geological Significance of Fractal Dimensions

As mentioned above, the fractal dimension can be used as an effective quantitative characterization parameter for pore structure, gas adsorption, storage capacity, and pore complexity of shales in shale reservoir evaluations. $D1$ can reflect the gas adsorption and storage capacity of shales. Shales with larger $D1$ have a stronger gas adsorption capacity and are better natural gas reservoirs, especially for adsorbed gas. $D2$ can characterize pore structure complexity and heterogeneity. Shales with larger $D2$ have a higher proportion of micropores, more complex pore structures, and strong heterogeneity. All these will reduce the permeability of shales and make gas desorption and diffusion more difficult, thus impeding gas flow in the shale reservoir [14, 43–47]. Therefore, for evaluating shale gas potential, the larger the $D1$ value is, the better the reservoir properties of the shale, while $D2$ should be in the appropriate range to ensure that the reservoir is not too complex for exploitation. In the reservoir evaluation process, $D1$ should have a lower limit, and $D2$ should have an upper limit [22], such that a favorable reservoir characterized by fractal dimension would also have good gas adsorption, good storage capacity, and an acceptable pore structure complexity [48–51]. The gas content ratio of natural desorption (the sum of lost gas content and desorbed gas content) to the total gas content (the sum of lost gas content, desorbed gas content, and residual gas content) can be regarded as the approximate proportion of gas that can be produced naturally during the exploitation process (with no reservoir fracture reconstruction). Since the lost gas content is obtained mathematically, there is a certain error compared to the actual value. However, the ratio has a certain significance for the current analysis. A larger ratio means more gas produced naturally and lower exploitation difficulty [49, 52, 53]. Correlation between the ratio and $D2$ (Figure 11) indicates that when $D2$ exceeds 2.85, the proportion of desorbed gas tends to decrease.

Combined with isothermal adsorption test data, favorable reservoir evaluation criteria of Longtan shales in Guizhou can be formulated. The lower limit of $D1$ is set as 2.60. When $D1$ is less than 2.60, the gas adsorption and storage capacity of shale are insufficient. The upper limit of $D2$ is set as 2.85. When $D2$ is larger than 2.85, the proportion of desorbed gas in the shale decreases, and the pores become too complex. Consequently, gas productivity can be affected. When the clay mineral content of the shale is greater than 40.0% (Figure 9(a)) and the quartz content is less than 30.0% (Figure 9(b)), the shale brittleness is poor, which can hinder hydraulic fracturing [44]. Exploitation of this kind of shale ($D2 > 2.85$) requires a more detailed recoverability evaluation and complex fracture scheme.

7. Conclusions

(1) The characteristic fractal dimensions of marine-continental transitional Longtan shales in Guizhou are determined by piecewise fitting based on the FHH model. Fractal dimensions under low relative pressure ($P/P_0 \leq 0.5$) are recorded as $D1$ and range from 2.6655 to 2.8648 with an average value of 2.7426. Fractal dimensions under high relative pressure ($P/P_0 > 0.5$) are recorded as $D2$ and range from 2.6841 to 2.9256 with an average value of 2.7838. High $D1$ and $D2$ values (closer to 3) indicate that the Longtan shales in Guizhou have good gas storage capacity and complex pore structures

(2) Both $D1$ and $D2$ show positive correlations with specific surface areas and negative correlations with pore size. $D1$ also shows a good positive correlation with the maximum gas absorption capacity of the shale. $D1$ and $D2$ increase with increasing organic matter and have complex correlations with organic maturity. There are positive correlations between fractal dimensions and clay mineral content and pyrite content, as well as a negative correlation between fractal dimensions and quartz content

(3) For the set of marine-continental transitional shales of the Longtan Formation in Guizhou, the lower limit of $D1$ is set as 2.60, and the upper limit of $D2$ is set as 2.85. When $D1$ is less than 2.60, the gas adsorption and storage capacity of the shale are insufficient. When $D2$ is larger than 2.85, the shale pores are so complex that the permeability is poor and natural productivity is low, indicating that the recoverability of the shale reservoir requires further evaluation

Data Availability

The data used to support the findings of this study are included within the article and are available from the corresponding author upon request.

Conflicts of Interest

The authors declare that they have no conflicts of interest.

Acknowledgments

This research was jointly supported by the Technical Fund Project of the Guizhou Science and Technology Department (QKHJC No.[2019]1293), Fund Project of the Education Department of Guizhou Province (QJH No.KY [2018]029), Fund Program of the Science and Technology Department of Liupanshui City (52020-2018-03-03), and Fund Program of the Science and Technology Department of Liupanshui City (52020-2019-05-03).

References

[1] J. Zhang, X. Li, G. Zhang, X. Zou, F. Wang, and Y. Tang, "Microstructural investigation of different nanopore types in marine-continental transitional shales: examples from the Longtan formation in southern Sichuan Basin, South China," *Marine and Petroleum Geology*, vol. 110, pp. 912–927, 2019.

[2] T. Cao, H. Xu, G. Liu, M. Deng, Q. Cao, and Y. Yu, "Factors influencing microstructure and porosity in shales of the Wufeng-Longmaxi formations in northwestern Guizhou, China," *Journal of Petroleum Science and Engineering*, vol. 191, article 107181, 2020.

[3] D. Avnir and M. Jaroniec, "An isotherm equation for adsorption on fractal surfaces of heterogeneous porous materials," *Langmuir*, vol. 5, no. 6, pp. 1431–1433, 1989.

[4] J. Chen, G. Y. Zhou, X. L. Zhao, and C. He, "Overview of study methods of reservoir rock pore structure," *Special Oil and Gas Reservoirs*, vol. 12, no. 4, pp. 11–14, 2005.

[5] D. Zhao, S. Yin, Y. Guo et al., "Investigation of pore structure characteristics of marine organic-rich shales using low-pressure N2 adsorption experiments and fractal theory," *Interpretation*, vol. 7, no. 3, pp. T671–T685, 2019.

[6] J. C. Zhang, Z. J. Jin, and M. S. Yuan, "Reservoiring mechanism of shale gas and its distribution," *Natural Gas Industry*, vol. 24, no. 7, pp. 15–18, 2004.

[7] C. Zou, D. Dong, S. Wang et al., "Geological characteristics and resource potential of shale gas in China," *Petroleum Exploration and Development*, vol. 37, no. 6, pp. 641–653, 2010.

[8] Q. Bai, S. G. Liu, W. Sun et al., "Reservoir characteristics of Wufeng Formation Longmaxi Formation in southwest of Sichuan Basin, China," *Journal of Chengdu University of Technology: Science & Technology Edition*, vol. 40, no. 5, pp. 521–531, 2013.

[9] T. Cao, Z. Song, H. Luo, Y. Zhou, and S. Wang, "Pore system characteristics of the Permian transitional shale reservoir in

the lower Yangtze region, China," *Natural Gas Geoscience*, vol. 1, no. 5, pp. 383–395, 2016.

[10] C. Bi, J. Q. Zhang, Y. S. Shan et al., "Geological characteristics and co-exploration and co-production methods of Upper Permian Longtan coal measure gas in Yangmeishu Syncline, Western Guizhou Province, China," *China Geology*, vol. 3, no. 1, pp. 38–51, 2020.

[11] P. Zhang, J. C. Zhang, Y. Q. Huang, X. Tang, Z. P. Wang, and J. J. Peng, "Characteristics and gas content evaluation of Wufeng-Longmaxi formation shale in Well Xiye-1," *Resources & Industries*, vol. 17, no. 4, pp. 48–55, 2015.

[12] C. R. Clarkson, N. Solano, R. M. Bustin et al., "Pore structure characterization of north American shale gas reservoirs using USANS/SANS, gas adsorption, and mercury intrusion," *Fuel*, vol. 103, pp. 606–616, 2013.

[13] M. Mastalerz, A. Schimmelmann, A. Drobniak, and Y. Chen, "Porosity of Devonian and Mississippian New Albany Shale across a maturation gradient: insights from organic petrology, gas adsorption, and mercury intrusion," *AAPG Bulletin*, vol. 97, no. 10, pp. 1621–1643, 2013.

[14] Y. Cai, D. Liu, Z. Pan, Y. Yao, J. Li, and Y. Qiu, "Pore structure and its impact on CH4 adsorption capacity and flow capability of bituminous and subbituminous coals from Northeast China," *Fuel*, vol. 103, pp. 258–268, 2013.

[15] X. Liu, J. Xiong, and L. Liang, "Investigation of pore structure and fractal characteristics of organic-rich Yanchang formation shale in central China by nitrogen adsorption/desorption analysis," *Journal of Natural Gas Science and Engineering*, vol. 22, pp. 62–72, 2015.

[16] M. Wang, H. Xue, S. Tian, R. W. T. Wilkins, and Z. Wang, "Fractal characteristics of upper cretaceous lacustrine shale from the Songliao Basin, NE China," *Marine and Petroleum Geology*, vol. 67, pp. 144–153, 2015.

[17] J. Hu, S. Tang, and S. Zhang, "Investigation of pore structure and fractal characteristics of the lower Silurian Longmaxi shales in western Hunan and Hubei provinces in China," *Journal of Natural Gas Science and Engineering*, vol. 28, pp. 522–535, 2016.

[18] J. Pan, K. Wang, Q. Hou, Q. Niu, H. Wang, and Z. Ji, "Micropores and fractures of coals analysed by field emission scanning electron microscopy and fractal theory," *Fuel*, vol. 164, pp. 277–285, 2016.

[19] Guizhou Provincial Bureau of Geology and mineral resources, *Regional geology of Guizhou Province*, Geological Publishing House, Beijing, 1987.

[20] R. Chen, K. Yuan, Z. Y. Zhang, and Q. F. Xu, "Sedimentary environment of organic-rich shale in the Upper Permian Longtan Formation in Qinglong area, western Guizhou, China," *China Geology*, vol. 2, no. 1, pp. 108-109, 2019.

[21] X. Ma and S. Guo, "Comparative study on shale characteristics of different sedimentary microfacies of Late Permian Longtan Formation in Southwestern Guizhou, China," *Minerals*, vol. 9, no. 1, p. 20, 2019.

[22] P. Zhang, Y. Q. Huang, H. Y. Liu, and J. W. Yang, "Fractal characteristics of the Longtan formation transitional shale in Northwest Guizhou," *Journal of China Coal Society*, vol. 43, no. 6, pp. 1580–1588, 2018.

[23] K. S. W. Sing, "Evaluation of the fractal dimension from a single adsorption isotherm," *Langmuir*, vol. 11, no. 6, pp. 2316-2317, 1995.

[24] S. B. Han, J. C. Zhang, C. Yang et al., "The characteristics of nanoscale pore and its gas storage capability in the lower Cambrian shale of Southeast Chongqing," *Journal of China Coal Society*, vol. 38, no. 6, pp. 1038–1043, 2013.

[25] F. Yang, Z. F. Ning, Q. Wang, D. T. Kong, K. Peng, and L. F. Xiao, "Fractal characteristics of nanopore in shales," *Natural Gas Geo Science*, vol. 25, no. 4, pp. 618–623, 2014.

[26] F. Yang, Z. Ning, and H. Liu, "Fractal characteristics of shales from a shale gas reservoir in the Sichuan Basin, China," *Fuel*, vol. 115, pp. 378–384, 2014.

[27] Z. W. Wang, S. F. Lu, M. Wang, and S. S. Tian, "Fractal characteristic of lacustrine shale and marine shale. Lithologic reservoirs," *Lithologic Reservoirs*, vol. 28, no. 1, pp. 88–93, 2016.

[28] Y. D. Xi, S. H. Tang, J. Li, and L. Li, "Investigation of pore structure and fractal characteristics of marine-continental transitional shale in the east central of Qinshui Basin," *Natural Gas Geoscience*, vol. 28, no. 3, pp. 366–376, 2017.

[29] J. Xiong, X. Liu, and L. Liang, "An investigation of fractal characteristics of marine shales in the southern China from nitrogen adsorption data," *Journal of Chemistry*, vol. 2015, 12 pages, 2015.

[30] J. Xiong, X. J. Liu, L. X. Liang, and T. Wu, "On the differences of reservoir characteristics of the upper and the lower Longmaxi Formation shale in the Changning region of Sichuan Basin," *Journal of Northwest University: Natural Science Edition*, vol. 45, no. 4, pp. 623–630, 2015.

[31] L. Liang, J. Xiong, and X. Liu, "An investigation of the fractal characteristics of the upper Ordovician Wufeng Formation shale using nitrogen adsorption analysis," *Journal of Natural Gas Science and Engineering*, vol. 27, pp. 402–409, 2015.

[32] P. Pfeifer and D. Avnir, "Chemistry in noninteger dimensions between two and three. I. Fractal theory of heterogeneous surfaces," *The Journal of Chemical Physics*, vol. 79, no. 7, pp. 3558–3565, 1983.

[33] Z. D. Li, J. L. Zhou, H. Wen, and N. Sun, "Characteristics of reservoir in northern Beixixiepo area of Hailar Basin and their influencing factors," *Acta Petrologica et Mineralogica*, vol. 27, no. 1, pp. 45–51, 2008.

[34] . Xue, J. C. Zhang, C. Yang, X. J. Man, and W. Dang, "Characteristics of microscopic pore and gas accumulation on shale in Longmaxi Formation, Northwest Guizhou," *Acta Petrolei Sinica*, vol. 36, no. 2, pp. 138–149, 2015.

[35] Y. M. Wang, D. Z. Dong, X. Z. Cheng, J. L. Huang, S. F. Wang, and S. Q. Wang, "Electric property evidences of the carbonfication of organic matters in marine shales and its geologic significance:a case of the Lower Cambrian Qiongzhusi Shale in southern Sichuan Basin," *Natural Gas Industry*, vol. 34, no. 8, pp. 1–7, 2014.

[36] I. R. Kaplan, K. J. Bird, and I. L. Tailleur, "Source of molten elemental sulfur and hydrogen sulfide from the Inigok well, northern Alaska," *AAPG Bulletin*, vol. 96, no. 2, pp. 337–354, 2012.

[37] Q. Zhang, R. H. Liu, Z. L. Pang, and W. Lin, "Pore fractal characteristics of Taiyuan formation shale in eastern uplift of Liaohe depression," *Geological Science and Technology Information*, vol. 35, no. 5, pp. 77–82, 2016.

[38] D. Li, C. H. Ou, Z. G. Ma, P. P. Jin, Y. J. Ren, and Y. F. Zhao, "Pyrite -shale interaction in shale gas enrichment and development," *Geophysical Prospecting for Petroleum*, vol. 57, no. 3, pp. 332–343, 2018.

[39] Z. B. Liu, B. Gao, Z. Q. Hu, W. Du, H. K. Nie, and T. Jiang, "Reservoir characteristics and pores formation and evolution of high maturated organic rich shale: a case study of Lower Cambrian Jiumenchong Formation, southern Guizhou area," *Acta Petrolei Sinica*, vol. 38, no. 12, pp. 1381–1389, 2017.

[40] T. T. Cao, M. Deng, Z. G. Song, G. X. Liu, Y. R. Huang, and A. S. Hursthouse, "Study on the effect of pyrite on the accumulation of shale oil and gas," *Natural Gas Geoscience*, vol. 29, no. 3, pp. 404–414, 2018.

[41] R. G. Loucks and S. C. Ruppel, "Mississippian Barnett shale: lithofacies and depositional setting of a deep-water shale-gas succession in the Fort Worth Basin, Texas," *AAPG Bulletin*, vol. 91, no. 4, pp. 579–601, 2007.

[42] Y. Zhang, J. C. Liu, H. Xu, X. L. Niu, G. H. Qin, and D. Y. Cao, "Comparison between pore structure and fractal characteristics of continental and transitional coal measures shale: a case study of Yan'an and Taiyuan formations at the northeastern margin of Ordos Basin," *Acta Petrolei Sinica*, vol. 38, no. 9, pp. 1036–1046, 2017.

[43] L. Chen, Z. X. Jiang, W. M. Ji et al., "Characteristics and significance of mineral compositions of fifth member of upper Triassic Xujiahe formation continental shale gas reservoir in western Sichuan depression," *Bulletin of Mineralogy, Petrology and Geochemistry*, vol. 35, no. 4, pp. 750–755, 2016.

[44] Z. Chong, Q. Yao, X. Li, L. Zhu, and C. Tang, "Effect of rock brittleness on propagation of hydraulic fractures in shale reservoirs with bedding-planes," *Energy Science & Engineering*, vol. 8, no. 7, pp. 2352–2370, 2020.

[45] J. J. Valenza II, N. Drenzek, F. Marques, M. Pagels, and M. Mastalerz, "Geochemical controls on shale microstructure," *Geology*, vol. 41, no. 5, pp. 611–614, 2013.

[46] J. Schieber, "Common themes in the formation and preservation of intrinsic porosity in shale and mudstones- illustrated with examples across the Phanerozoic," in *SPE Unconventional Gas Conference*, pp. 1–10, Pittsburgh, PA, USA, February 2010.

[47] J. C. Zhang, H. K. Nie, B. Xu, S. L. Jiang, P. X. Zhang, and Z. Y. Wang, "Geological condition of shale gas accumulation in Sichuan Basin," *Natural Gas Industry*, vol. 28, no. 2, pp. 151–156, 2008.

[48] J. L. Huang, D. Z. Dong, J. Z. Li, J. W. Hu, and Y. M. Wang, "Reservoir fractal characteristics of continental shale: an example from Triassic Xujiahe Formation shale, Sichuan Basin, China," *Natural Gas Geoscience*, vol. 27, no. 9, pp. 1611–1618,1708, 2016.

[49] Z. Sun, Y. Wang, Z. Wei et al., "Pore structure alteration characteristics of different mineralogical composition shale during shale-fracturing fluid physical-chemical interactions," *Geofluids*, vol. 2019, 13 pages, 2019.

[50] J. H. Li and B. Zheng, "A new method for fractal characterization of microscopic pores and its application in shale reservoirs," *Natural Gas Industry*, vol. 35, no. 5, pp. 52–59, 2015.

[51] L. Sun, Y. Q. Gao, Y. Pan, and C. H. Ou, "Surface fractal characteristics and their influence on shale nanopores," *Journal of Southwest Petroleum University(Science & Technology Edition)*, vol. 39, no. 6, pp. 85–91, 2017.

[52] S. F. Wang, C. N. Zou, D. Z. Dong, Y. M. Wang, J. L. Huang, and S. J. Guo, "Biogenic silica of organic-rich shale in Sichuan Basin and its significance for shale gas," *Acta Scientiarum Naturalium Univesitatis Pekinensis*, vol. 50, no. 3, pp. 476–486, 2014.

[53] Y. Yang and A. C. Aplin, "A permeability-porosity relationship for mudstones," *Marine and Petroleum Geology*, vol. 27, no. 8, pp. 1692–1697, 2010.